ELSEVIER

Spectrochimica Acta Part A 56 (2000) 363–371

SPECTROCHIMICA ACTA PART A

www.elsevier.nl/locate/saa

Filling factor of a paramagnetic sample in a rectangular cavity: theory and application

Aharon Blank *, Haim Levanon

Department of Physical Chemistry and the Farkas Center for Light-Induced Processes, The Hebrew University of Jerusalem, 91904 Jerusalem, Israel

Received 10 June 1999; accepted 17 September 1999

Abstract

A computational method is presented for calculating the filling factor of an electron paramagnetic resonance (EPR) tube in a rectangular TE_{102} cavity. The algorithm employs the conventional finite element method. In addition to the filling factor, the algorithm allows to calculate the quality factor and the reflection coefficient of the loaded cavity. This method allows calculating very accurately the EPR signal intensities from which the spin concentration of paramagnetic samples can be determined. A comparison between the predicted EPR signal intensities to several experimental results was found to be satisfactory. The method also allows optimizing the EPR tube dimensions and its glass quality to improve measurement sensitivity.

Keywords: Spin concentration determination; EPR; Numerical electromagnetic calculations

1. Introduction

Determination of spin concentration by EPR is of importance [1–3]. In such experiments, measurements of the number of unpaired spins are not possible without calibrating the instrument response relative to a known standard. The difficulty in using standards is that both the magnetic and dielectric properties of the sample should be taken into account. These properties are the magnetization (permeability, μ) and the dielectric constant (permittivity, ε). Although samples are usually placed about the node of the electric field, the specific dielectric properties still have a considerable effect on the electric and magnetic fields in the cavity. As a consequence, the filling and quality factors of the cavity (η and Q) are strongly dependent upon the specific sample inserted. This dependency must be taken into consideration when the concentration of spins of the reference and the unknown sample are required to be determined accurately.

The influence of the sample on the cavity's properties was treated semi-empirically in previous studies [1,4]. To the best of our knowledge, the most accurate approach was made by employing the 'field compression factor' method to describe the change in the magnetic field in the

* Corresponding author. Tel.: +972-2-6585544; fax: +972-2-5618033.

E-mail address: levanon@chem.ch.huji.ac.il (H. Levanon)

1386-1425/00/$ - see front matter
PII: S1386-1425(99)00247-4

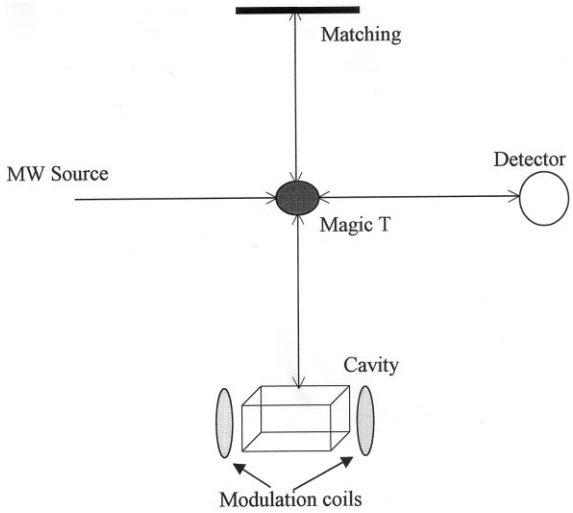

Fig. 1. Typical EPR instrumentation layout employed in the present study.

cavity upon sample insertion [1]. This method applies to the EPR experimental configuration shown in Fig. 1. Under such conditions, the field modulated EPR signal is proportional to [1]:

$$V = V_0 Q_L(\Gamma_2 - \Gamma_3)(1 + \Gamma_3)\left(\int_{V_s} B_1^2 B_2 \, dV / W_{st}\right) \quad (1)$$

where V_0 is the incident microwave voltage; Q_L is quality factor of the loaded cavity; Γ_2, Γ_3 are the reflection coefficients from the matched load and the cavity, respectively; B_1, B_2 are the microwave and modulation field amplitudes, respectively integrated over the sample volume (V_s); and W_{st} is the total energy stored in the cavity, which is given by:

$$W_{st} = \frac{1}{2}\int_{V_{cavity}} \frac{B_1^2}{\mu} \, dV \quad (2)$$

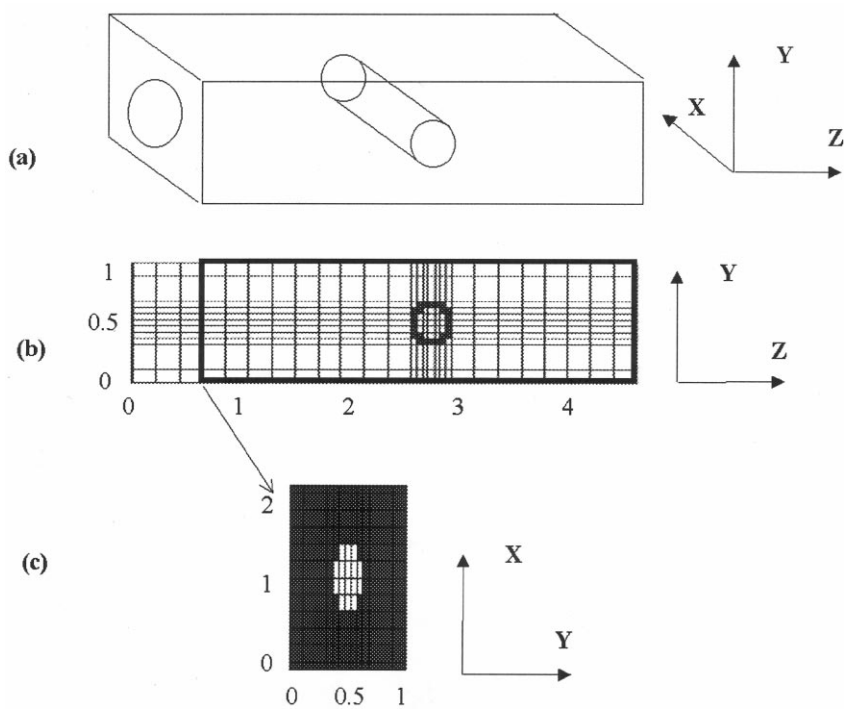

Fig. 2. Sample in a cavity as modeled by the FEM method (dimensions are in cm). (a) General 3-D view of the cavity with the cylindrical sample in it and the coupling iris; (b) FEM grid of the cavity and sample. The thick line represents cavity boundaries. The boundary conditions on the cavity are imposed by perfect conductor boundary conditions except for the coupling wall, which has a hole in it. An additional three segments are added before the cavity coupling wall and TE_{102} mode boundary conditions are imposed on the leftmost wall. The grid size is changed according to sample position; (c) The FEM representation of the iris.

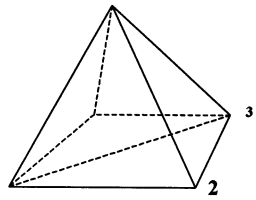

EDGE NO.	NODE 1	NODE 2
1	1	2
2	1	3
3	1	4
4	2	3
5	4	2
6	3	4

Fig. 3. The six edges of the tetrahedron defined in the numerical procedure. The electric fields are calculated along these edges.

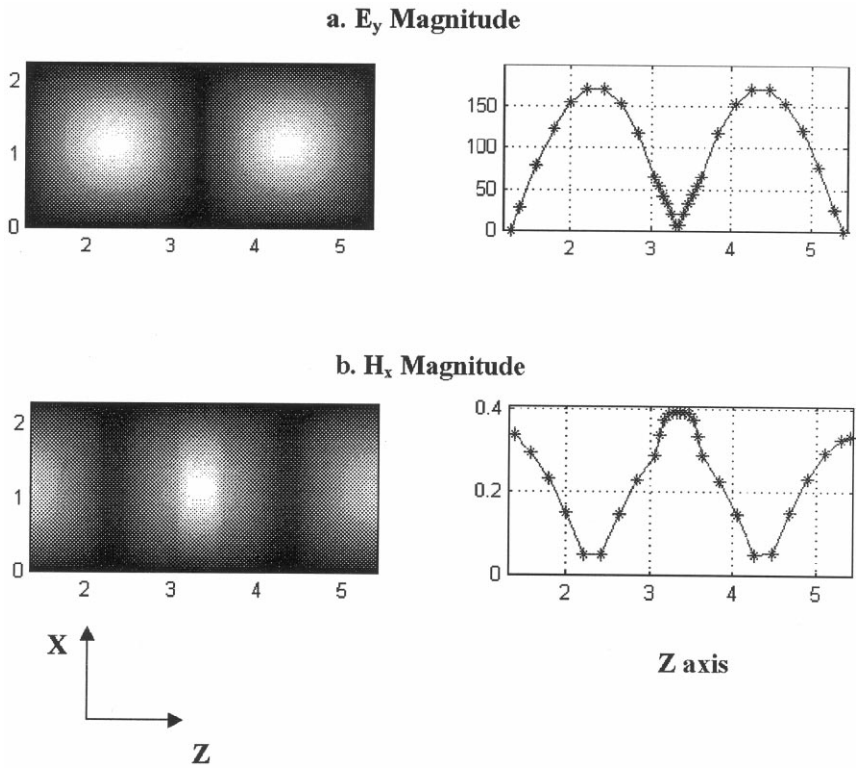

Fig. 4. Field distribution inside an X-band TE_{102} (1.016; 2.28; 4.15 cm) cavity with an empty quartz tube with inner radius of 2 mm, and outer radius of 3 mm. (a) The magnitude of E_y as a 2-D presentaTion in the $y = 0.5$ cm plane (left) and 1-D presentation along the z-axis of the cavity in $y = 0.5$ cm, $x = 1.15$ cm; (b) The magnitude of H_x as a 2-D presentation in $y = 0.5$ cm plane (left) and 1-D presentation along the z axis of the cavity in $y = 0.5$ cm, $x = 1.15$ cm. Notice the increase in magnetic field amplitude inside the tube.

Inspection of Eq. (1) shows that the EPR signal is directly proportional to the quantity $\zeta = \int_{V_s} B_1^2 B_2 \, dV$. Therefore, one can introduce the compression factor term, ψ (= [ζ(with sample)/ ζ(without sample)]), which describes the field compression when the sample is inside the cavity. Although the mathematical treatment associated with the compression factor is accurate, obtaining the actual quantity of this factor is complicated. This is because of the fact that EPR samples are usually placed along the long axis (x) of the rectangular cavity (Fig. 2a). Under such conditions, one can not derive exact analytical expressions for calculating ψ, since the problem becomes a three-dimensional, with no separable wave equation. However, if the sample is placed along

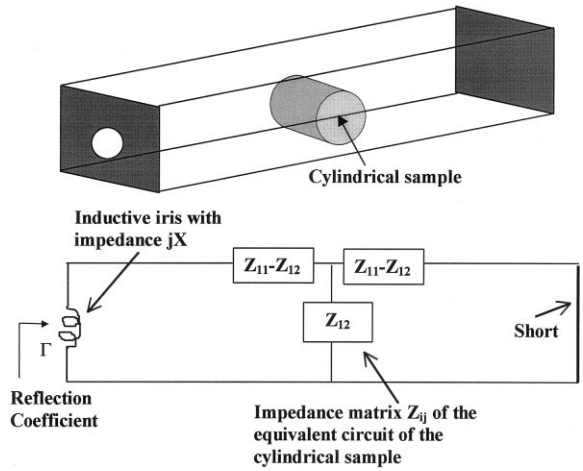

Fig. 5. Schematic presentation of the cavity and sample (top) and its transmission lines analogous representation (bottom).

the y-axis, the two-dimensional symmetry of the TE_{102} mode in the cavity is not broken and one can derive, by the variational principle, a rather accurate closed form expression for the field inside the sample [5]. The case where the sample is inserted along the z-axis of the cavity is not practical, experimentally and computationally. In most EPR cavities the sample is inserted along the x-axis. Thus, one is left with two possibilities:

1. Empirical measurement of the compression factor for different tube dimensions, solvents, etc., as was carried out by Casteleijn [1] with a small DPPH grain in the middle of the sample or;
2. the method we introduce here that is much more general and accurate, which uses numerical calculations of the electromagnetic (EM) fields inside the cavity.

Remarkable progress has been achieved in recent years in the field of computational electromagnetics, which models and solves numerically the electromagnetic fields in variety of structures [6]. Computational electromagnetic techniques were previously used to design new EPR cavity structures [7], and general purpose commercial computational electromagnetic software is now widespread [8]. In spite of the existence of such commercial general-purpose codes, we saw the importance of introducing new software for solving the specific problem that was described above. This software is more efficient than general-pur-

Table 1
Comparison between calculated and experimental EPR results for a point sample inside a quartz tube with several tube dimensions

d_o/d_i[a] (mm)	Δf of resonance frequency[b] (MHz)		η_{calc}[c] (normalized)	Q_{calc}[d]	T_{calc}[e]	r_{couple}[f] (mm)	EPR signal[g] (normalized)	
	[17]	Calc.					[17]	Calc.
Empty	0	0	1	1000	0.95	4.41	1	1
4.0/2.9	15	12	1.13	999.37	~1	4.88	1.2	1.19
5.2/3.6	32	36	1.234	998.30	~1	4.94	1.30	1.29
9.3/8.5	99	110	1.14	993.3	~1	4.72	1.32	1.19
4.3/1.1	22	26	1.361	998.12	~1	4.87	1.32	1.42
7.4/5.6	94	114	1.41	993.37	~1	4.95	1.41	1.47
6.6/1.3	94	121	1.71	993.5	~1	5.21	1.77	1.79

[a] Inner and outer diameters of the tube (in mm).
[b] Measured and calculated frequency shift of the cavity relative to empty cavity.
[c] Normalized filling factor (relative to empty cavity).
[d] Calculated quality factor of the cavity with the tube, assuming an empty cavity $Q = 1000$.
[e] Calculated transmission coefficient into the cavity $(1+\Gamma)$.
[f] Calculated coupling radius of iris to achieve critical coupling.
[g] Calculated and measured EPR signal relative to an empty cavity. The calculated EPR signal is ηQT.

Table 2
Calculated and experimental results of EPR signal intensity of DPPH in various solvents

Solvent	$\varepsilon'/\varepsilon_0$	tan δ $\times 10^4$	η	Q_L	T	ηQT[a]	EPR signal[b]
Toluene	2.24	10	0.042985	599.2	0.973	1	1
Ethanol	1.7	680	0.0423	569.37	0.921	0.88	0.86
Methanol	8.9	8100	0.0509	141.05	0.934	0.295	0.31
Carbon tetrachloride	2.17	16	0.0428	598.89	0.972	0.99	0.98

[a] This calculated quantity is proportional to the EPR signal and is normalized to the signal of DPPH in toluene.
[b] This measured quantity is normalized to toluene.

pose codes and includes algorithms, which enables the use of optimized tube dimensions to gain maximum signal sensitivity. An additional problem that the code handles, and which is not addressed by general computational electromagnetics codes, is a numerical mimicry of the process of cavity matching. Namely, for different sample properties, the cavity's matching iris dimensions must be changed to achieve critical coupling.

2. The Numerical Algorithm

The numerical algorithm, which was used to calculate the EM fields inside a rectangular cavity with an inserted sample is based on the finite element method (FEM) technique [9,10] with the specific approach developed by Ali [11]. The FEM technique is based on a numerical solution of the 'weak representation' of the electromagnetic wave equation. This approach starts with the three-dimensional wave equation:

$$\nabla \times \left(\frac{1}{\mu_r(\mathbf{r})} \nabla \times \mathbf{E}(\mathbf{r}) \right) - k_0^2 \varepsilon_r(\mathbf{r}) \mathbf{E}(\mathbf{r}) = -jk_0 Z_0 \mathbf{J}(\mathbf{r}) \tag{3}$$

where μ_r is the permeability, which can be a function of the space coordinates ($\mathbf{r}$); $\mathbf{E}$ is the electric field vector; k_0 is the free-space wave number ($2\pi/\lambda$); ε_r is the permittivity; Z_0 is free space impedance (about 377 Ω); and $\mathbf{J}$ is the vector of an electric current source.

Numerical manipulation of this equation results in the linear set of equations:

$$[A_{mn}][E_n] = [R_m] \tag{4}$$

where:

$$A_{mn} = \int_V \left[\frac{1}{\mu_r} (\nabla \times \mathbf{w}_n(\mathbf{r})) \cdot (\nabla \times \mathbf{w}_m(\mathbf{r})) - jk_0 Z_0 \varepsilon_r \mathbf{w}_n(\mathbf{r}) \cdot \mathbf{w}_m(\mathbf{r}) \right] \mathrm{d}V$$

and

$$R_m = -jk_0 Z_0 \left[\int_V [\mathbf{J}_m(\mathbf{r})] \cdot \mathbf{w}_m(\mathbf{r}) \, \mathrm{d}V - \oint_S \mathbf{J}_m(\mathbf{r}) \cdot \mathbf{w}_m(\mathbf{r}) \, \mathrm{d}S \right]$$

where n and m are indices which cover all the discrete volumes of the relevant space (Appendix A).

Since most of the theory behind this derivation appears only in a recent Ph.D. dissertation [11], we provide the reader with a detailed discussion in the Appendix A. Nevertheless, we can give some basic physical insight of Eq. (4), which represents a linear relation between the electric fields at specific points in space (matrix $\mathbf{A}$ in Eq. (4)). Thus, the numerical algorithm, by dividing the space into small volumes, allows the electric fields to be obtained at any point (vector $\mathbf{E}$ in Eq. (4)) because of arbitrary excitation (vector $\mathbf{R}$ in Eq. (4)). The algorithm divides the relevant space into tetrahedrons (Fig. 3) and each tetrahedron can have it's own electromagnetic properties (ε_r and μ_r).

The solution of this linear system of equations is made by an iteration procedure to finally obtain the electric field at all nodes. With this field information all the electromagnetic properties of the cavity, whether it is empty or occupied by a sample, can be calculated. It is important to emphasize that although the fields are calculated in a tetrahedron structure, the algorithm uses rectan-

gular boxes (hexahedrons) to define the geometry of the structure, which later are divided into tetrahedrons (five tetrahedrons in each hexahedron). The results are also reported per hexahedron.

3. Applications

3.1. Determination of spin concentrations by EPR

As was noted in the introduction, accurate determination of spin concentrations by EPR experiments suffers from the fact that the reference and unknown samples usually don't have similar permittivity. This problem was demonstrated in a recent experiment, where measurements of the same samples with different standards resulted in different results [2]. It should be pointed out that the experiments were carried out without taking into account the different permittivity values of the various standards. The inconsistencies in the results between those experiments were substantial. These discrepancies can be accounted for as a result of not taking into account the permittivity differences, which can easily affect the accuracy within the order of 50–100% [1].

To account for permittivity differences, one can use the semi-empirical 'field compression factor' method. However, acquiring this factor requires elaborated measurements, which may themselves be very inaccurate. Therefore, without any simple computational procedure in hand, the effects of the differences in the permittivity of the sample and standard are rarely considered. This is why and where the numerical electromagnetic calculation can make its substantial contribution.

We describe bellow the application of our numerical procedure to treat these types of problems. By neglecting the influence of field modulation Eq. (1), and assuming constant incident microwave power and matching (V_0 and $\Gamma_2 - \Gamma_3$ are constant) the EPR signal is proportional to $Q_L \eta T$, where T is the transmission coefficient of the cavity (namely, $T = 1 + \Gamma_3$) and η is the filling factor with its conventional definition [12]. Calculation of η and Q_L of the cavity, requires accurate knowledge of the electric and magnetic fields' distribution inside the cavity. However, these fields distribution does not depend upon the way the cavity is being excited. In other words, the fields at resonance are eigen modes of a specific cavity and sample structure. This fact enables to treat the problem with a very compact close structure in terms of the FEM formulation, as shown in Fig. 2b. Most of the computational domain is the cavity itself, and only several hexahedrons which are outside the cavity, are needed for coupling the microwave source to the cavity. Fig. 2b presents an additional feature, which is unique to the FEM formulation, and enables the use of an adjustable hexahedron grid size. With this feature, the number of unknowns is reduced and the thin tubes inside the cavity can be modelled accurately and efficiently.

The results of such calculations are presented in Fig. 4. It can be seen that one can obtain complete knowledge of the electric and magnetic fields distribution in the cavity. After having calculated the electric and magnetic fields, the filling factor can be obtained by Eq. (5):

$$\eta = \frac{\sum_n (H_x^{n2} + H_z^{n2}) \cdot V_n}{\sum_m (H_x^{m2} + H_z^{m2}) \cdot V_m} \tag{5}$$

where n is an index running over all the hexahedrons of which the sample volume consists of, and m is an index running over all hexahedrons of the entire cavity; and V_n is the volume of the nth hexahedron. We take into account only H_x and H_z because H_y is usually negligible (although, if required, it can be easily taken into to the calculation). We should also note that we consider H and not B because we assume that the permeability is of free space, even in the sample. Inspection of Fig. 4, shows that inserting an empty tube inside the cavity causes the magnetic field to become stronger inside the tube volume (i.e., the compression factor is larger than 1). In addition, the z-dependency of the field is smaller inside the tube (the field is almost constant with respect to the z-axis).

As noted above, for most EPR spectrometers, the signal is proportional to $Q_L \eta T$. Thus, full use

of this computational method, for determining the spin concentration in EPR experiments, can be made only if we can calculate the change in Q and T as a result of inserting different samples into the cavity. The empty cavity quality factor, Q_e, can be measured by network analyzer [13], or by measurement of the ringing time after a microwave pulse (by the equation $Q = \nu_0^e/\pi\tau_R$, where ν_0^e is the resonance frequency of the empty cavity and τ_R is the ringing characteristic time of the cavity). Once the empty cavity Q_e is known, we can calculate the total Q_L (cavity and sample), through our knowledge of the electric and magnetic fields in the cavity:

$$Q_L = \left(\frac{\sum_m \varepsilon''_m (E_y^{m2} + E_y^{m2} + E_y^{m2}) \cdot V_m}{\sum_m (H_x^{m2} + H_z^{m2}) \cdot V_m} + 1/Q_e \right)^{-1} \quad (6)$$

where the summation is on the entire cavity volume. Note that ε''_m (the imaginary part of the permittivity) depends on the cell index, i.e. the position in the cavity.

The resonance frequency of the cavity obviously changes as the sample is inserted. Therefore, in order to find the new resonance frequency, the calculation of Q_L (and η) is repeated several times (typically, ten times) until the results converge to the new resonance frequency of the loaded cavity (ν_0^L). The new resonance frequency is also an important factor that comes out of the calculation. At this frequency, the final results of η, Q_L and T are obtained.

Unlike the calculation of Q_L and η (in a finite closed domain), the calculation of T requires an open domain. The accurate calculation of T is important, because as different samples are inserted in the cavity, it's reflection coefficient, Γ_3, changes, and as mentioned above, $T = 1 + \Gamma_3$. Finding Γ_3 is not trivial, because in every CW EPR measurement, the goal is to minimize Γ_3 by changing the matching properties of the cavity (i.e. to achieve critical coupling). We have found that the analogous numerical-computational of the cavity matching may be described by the following procedure:

1. After Q_L, η and ν_0^L are found, we calculate the impedance matrix of the sample in the cavity. This impedance matrix is shown in Fig. 5 and is the general form of a symmetric four-terminal microwave network [14]. The calculation of the impedance matrix is made at the resonance frequency by employing the FEM procedure.
2. The impedance matrix of the coupling iris can be calculated by a closed form expression given elsewhere [14]. This calculation is done for several iris diameters and, for each case, the reflection coefficient of the whole structure (shown in Fig. 5 in transmission lines representation) can be evaluated by standard transmission lines theory. The iris radius, which corresponds to the minimal reflection coefficient, is chosen as the matching iris radius.

With the above numerical procedure, the EPR signal, which is proportional to $Q_L\eta T$ is obtained.

3.2. Signal to noise optimization

We have shown how to calculate the factor $Q_L\eta T$ that is proportional to the EPR signal. Once this factor is known, it is possible to optimize the signal-to-noise-ratio (SNR), namely, to increase the EPR signal by maximizing $Q_L\eta T$. The variables, which can be changed by our program, are the tube's inner and outer diameters, keeping other variables, such as solvent properties, cavity dimensions, etc., fixed. The optimization can be carried out by several methods. Here, we have employed the Nedler-Mead simplex search method [15,16]. For example, we optimized the quartz tube dimensions of a paramagnetic sample dissolved in toluene, in a standard TE_{102} mode cavity. The calculated optimal tube dimensions are 4.2 and 4.8 mm for the inner and outer radii, respectively. The optimized inner and outer radii of the EPR tube will, of course, depend on the sample and tube dielectric properties (quartz, pyrex, etc.), and the cavity's dimensions. It is clear that for different cavities and different samples, the optimized tube dimensions are different.

4. Numerical and Experimental Examples

To verify our calculations, based upon Ali's approach [11], we have compared our numerical results to those available in the literature and to experimental data gained in our study. Let us first consider the experiment where a point sample (DPPH) in a quartz tube was measured to acquire the variations in the EPR signal intensity as a function of the tube thickness [17]. The comparison of these results with our calculations is given in Table 1. It can be seen that changing tube dimensions can result in substantial changes in the EPR signal intensity, which is followed closely by the numerical calculations.

The second example emphasizes the importance of using our approach in the determination of spin concentration. As a reference, we have used a small amount of DPPH, which was dissolved in different solvents, i.e. ethanol, methanol, carbon tetrachloride and toluene (≈ 1 mM). All measurements were taken shortly after sample preparation. The permittivity of the solvents at X-band frequency, was obtained from known data [18], and assuming that the DPPH effect on the solvent permittivity is negligible. With a paramagnetic sample or solution whose permittivity in the microwave regime is unknown, there are several methods of determining this value [13]. Measurements were made with an X-band CW spectrometer (Varian model E-LINE) in a TE_{102} cavity ($1.02 \times 2.29 \times 4.15$ cm), and 100 mW microwave power. Quality factor of the empty cavity was measured by the ringing time of the cavity, after a strong microwave pulse using a Bruker pulsed spectrometer (ESP 380E). The Q of the empty cavity was found to be ≈ 600. Solvents were placed in a quartz tube with an inner radius of 1.5 mm and an outer radius of 2 mm (with no finger dewer). The results were digitized and integrated twice, and were compared to the calculated ones as shown in Table 2. Again, it can be seen that the solvent properties can substantially affect the cavity's Q, η and Γ_3, which results in differences in the EPR signal intensity of the same amount of spins.

5. Conclusions

We have presented a new computational method to calculate the electromagnetic properties of a rectangular EPR cavity loaded with a dielectric sample. The method should be used when accurate knowledge of the number of unpaired spins in the sample is required. The numerical algorithm is versatile and accurately models an EPR measurement. In other words, when a new sample is inserted in the cavity, the frequency is swept to find the new resonance frequency. In addition, the iris changes its dimensions to achieve the new critical coupling. Finally, at resonance frequency and the optimal iris radius, the EPR signal is calculated. Comparison with several EPR measurements was found to be satisfactory.

Acknowledgements

This work is in partial fulfilment of the requirements for a Ph.D. degree (A.B.) at the Hebrew University of Jerusalem. This work was partially supported by the Israel Ministry of Science, through the 'Eshkol Foundation' (A.B.), by a US-Israel BSF grant and by the Volkswagen Foundation (I/73-145). The Farkas Research Center is supported by the Bundesministerium für die Forschung und Technologie and the Minerva Gesellschaft für Forchung GmbH, FRG. We are also grateful to Professor Todd Hubing (University of Missouri-Rolla), for providing us with his FEM software.

Appendix A. Derivation of the numerical linear equations in the FEM formulation

We begin by multiplying Eq. (3) (in the main text) by a vector weighing function, $\mathbf{w}(\mathbf{r})$, and integrate over the volume V to obtain the 'weak form of the wave equation':

$$\int_V \left[\nabla \times \left(\frac{1}{\mu_r} \nabla \times \mathbf{E}(\mathbf{r}) \right) \cdot \mathbf{w}(\mathbf{r}) - k_0^2 \varepsilon_r \mathbf{E}(\mathbf{r}) \cdot \mathbf{w}(\mathbf{r}) \right] \mathrm{d}V = -jk_0 Z_0 \int_V [\mathbf{J}(\mathbf{r})] \cdot \mathbf{w}(\mathbf{r}) \, \mathrm{d}V \quad \text{(A1)}$$

Using the Green's first vector theorem we can derive:

$$\int_V \left[\left(\frac{1}{\mu_r} \nabla \times \mathbf{E}(\mathbf{r}) \right) \cdot (\nabla \times w(\mathbf{r})) - k_0^2 \varepsilon_r \mathbf{E}(\mathbf{r}) \cdot \mathbf{w}(\mathbf{r}) \right] \mathrm{d}V =$$

$$= -jk_0 Z_0 \left[\int_V [\mathbf{J}(\mathbf{r})] \cdot \mathbf{w}(\mathbf{r})\, \mathrm{d}V - \oint_S \mathbf{J}(\mathbf{r}) \cdot \mathbf{w}(\mathbf{r})\, \mathrm{d}S \right] \quad \text{(A.2)}$$

where S is the surface enclosing the volume V.

The electric field and the vector function $\mathbf{w}$ are modeled by sub-domain function $\mathbf{w}_k(\mathbf{r})$ is defined on separate tetrahedrons as:

$$\mathbf{w}_k(\mathbf{r}) = \begin{cases} \mathbf{f}_k + \mathbf{g}_k \times \mathbf{r} & r \quad inside \quad tetrahedron \\ 0 & r \quad outside \quad tetrahedron \end{cases}$$

where:

$$\mathbf{f}_k = \frac{b_k}{6V_e} (\mathbf{r}_{(7-k)1} \times \mathbf{r}_{(7-k)2})$$

$$\mathbf{g}_k = \frac{b_k b_{(7-k)}}{6V_e} \mathbf{e}_{(7-k)}$$

k, 1...6 (The six edges of the tetrahedron as defined in Fig. 3); V_e, volume of the tetrahedron; $\mathbf{e}_k$, unit vector of the kth edge; b_k, length of the kth edge; $\mathbf{r}_{ij}$, position of the point j (1 or 2) at the ith edge.The electric field $\mathbf{E}$ within the volume V_q of the tetrahedron can be expanded as:

$$\mathbf{E}(\mathbf{r}) = \sum_{i=1}^{6} E_i^q \mathbf{w}_i(\mathbf{r}) \quad \text{(A.3)}$$

where $\{E_i^q\}$ is a set of unknown complex scalar coefficients which are yet to be found. Inserting the expression for $\mathbf{E}(\mathbf{r})$ of Eq. (A.3) into Eq. (A.2) will give a discreet form of Eq. (A.3) as a matrix solution (Eq. (4) detailed in the main text):

$$[A_{mn}][E_n] = [R_m] \quad \text{(A.4)}$$

References

[1] G. Casteleijn, J.J. Ten Bosch, J. Smith, J. Appl. Phys. 39 (1968) 4375.
[2] N.D. Yordanov, Appl. Magn. Res. 6 (1994) 333.
[3] R. Czoch, Appl. Magn. Res. 10 (1996) 293.
[4] M. Mazur, M. Valko, H. Morris, R. Kleement, Anal. Chemic. Acta 333 (1996) 253.
[5] J. Schwinger, D. Saxon, Discontinuities in Waveguides, Gordon and Breach Science, New York, 1968.
[6] A.F. Peterson, S.L. Ray, R. Mittra, Computational Methods for Electromagnetics, Oxford University Press, Oxford, 1998.
[7] S. Pfenninger, J. Forrer, A. Schweiger, T.H. Weiland, Rev. Sci. Instrum. 59 (5) (1988) 752.
[8] ANSOFT, ANSYS, Commercial EM codes are available.
[9] J. Jianming, The Finite Element Method in Electromagnetic, John Wiley, New York, 1993.
[10] J. Volakis, A. Chatterjee, L. Kempel, Finite Element Method for Electromagnetics, IEEE Press, New Jersey, 1998.
[11] M.W. Ali, Ph.D. Dissertation, University of Missouri-Rolla, 1996.
[12] C.P.J. Poole, Dover Publication, Mineola, NY, 1996 (Chapter 5).
[13] M. Sucher, J. Fox, Handbook of Microwave Measurements, Polytechnic Press, 1970.
[14] N. Marcuvitz, Waveguide Handbook, McGraw-Hill, 1951.
[15] J.A. Nelder, R. Mead, Comput. J. 7 (1991) 308.
[16] J.E.J. Dennis, D.J. Woods, in: A. Wouk (Ed.), Microcomputers in Large-Scale Computing, SIAM, 1987, p. 116.
[17] N.D. Yordanov, P. Slavov, Appl. Magn. Res. 10 (1996) 351.
[18] A.R. Von Hippel, Dielectric Materials and Applications, MIT Press, 1959.